Applied Surface Science 532 (2020) 147397

Contents lists available at ScienceDirect

Applied Surface Science

journal homepage: www.elsevier.com/locate/apsusc

Broadband omnidirectional antireflection coatings inspired by embroidered ball-like structures on leafhoppers

Meng-Shan Shih, Huei-Yin Chen, Pei-Chun Li, Hongta Yang*

Department of Chemical Engineering, National Chung Hsing University, 145 Xingda Road, Taichung City 40227, Taiwan

ARTICLE INFO

Keywords:
Leafhopper
Brochosomes
Embroidered ball-like structures
Omnidirectional antireflection
Langmuir-Blodgett technology

ABSTRACT

Leafhopper (*Thaia rubiginosa*) wings exhibit antireflection behaviors for wide viewing angles, resulting from leafhopper-generated brochosomal coatings on the wing surface. The embroidered ball-like brochosomes establish a gradual transition in the refractive index at air/wing interface, leading to the broadband omnidirectional antireflection performance. Inspired by the brochosomal coatings, this study develops a non-photolithography-based approach for assembling embroidered ball-like structure arrays exploiting a modified Langmuir-Blodgett technology. The average visible transmittance of a polymer film can be improved by *ca.* 8% at normal incidence, and improved by even *ca.* 24% as the incident angle reaches 75° by introducing the artificial brochosome arrays. The dependence of the structure shape on the antireflection capabilities is also systemically studied in this research.

1. Introduction

Fresnel's reflection occurs as incident light penetrates through an air-material interface due to a refractive index mismatch between the two different media [1]. The light reflection from a material surface, accompanied with loss of light energy, possess strong glare and leads to vision impairment on optical devices. In view of this, numerous single-layer and multilayer antireflection coatings have been applied to suppress light reflection by rendering light destructive interferences [2,3]. Nevertheless, the traditional antireflection coatings suffer from narrowband antireflection performance with limited range of incident angles, rare choices of coating materials, and difficult assembly precision.

Over nearly four billion years, insects have evolved diverse lifestyles and features, such as high power of flight and highly transparent wings, which avoid being tracked by predators [4]. As we know, the subwavelength structures on transparent insect wings, including but not limited to cicada wings, dragonfly wings, and glasswing butterfly wings, eliminates light reflection and light scattering during flight by establishing a gradually changed refractive index on the surface of wings [5–7]. By gaining knowledge from the insect wings, a vast range of top-down photolithography-based technologies and methodologies have been developed to design and build cone arrays, nipple arrays, wire arrays, pyramid arrays, dome arrays, and hole arrays as antireflection coatings [8–14]. However, most of the technologies are limited by costly fabrication processes and low-resolution features. In contrary, bottom-up self-assembly technologies provide simple and inexpensive strategies to create antireflective structure arrays [15–19]. Unfortunately, the as-fabricated structures are provided with sharp refractive index transition, and thus cannot suppress the light reflection effectively [20–22].

To address the issues, a new non-photolithography-based methodology is developed to engineer hieratical structure arrays which inspired by leafhopper (*Thaia rubiginosa*, Motschulsky) wings in this study. The transparent leafhopper-produced brochosome-covered wings function as camouflage coatings to hide from their predators [23–25]. The brochosomes are submicrometer-scale granules covered with arranged subwavelength-scale holes, making the structural geometry similar to an embroidered ball [26]. The hierarchical structures behaving unique characteristics are promising for diverse applications in photoelectrochemical hydrogen production, biosensing fields, selective-superolephilic coatings, super-repellent coatings, and camouflage coatings [27–30]. Moreover, brochosome-like metal arrays are capable of suppressing reflection even as the incident angle reaches 45°, resulting from absorption by plasma excitations [31,32]. By electrodepositing metals onto micrometer-scale double-layer colloidal crystal templates, artificial brochosomes of the metal of choice can be fabricated. However, the introduction of micrometer-scale templates and the implantation of metals undoubtedly leads to a low transparency. Here, the leafhopper-produced brochosomal coatings with remarkable

* Corresponding author.
E-mail address: hyang@dragon.nchu.edu.tw (H. Yang).

https://doi.org/10.1016/j.apsusc.2020.147397
Received 22 April 2020; Received in revised form 26 July 2020; Accepted 27 July 2020
Available online 31 July 2020
0169-4332/ © 2020 Elsevier B.V. All rights reserved.

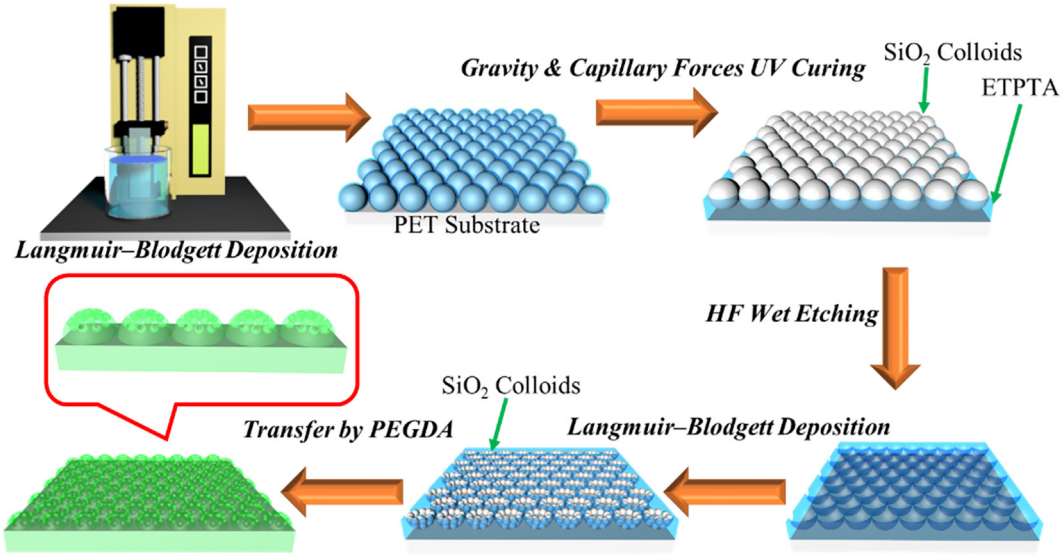

Fig. 1. Schematic illustration of the experimental procedure for fabricating leafhopper-inspired antireflection coatings.

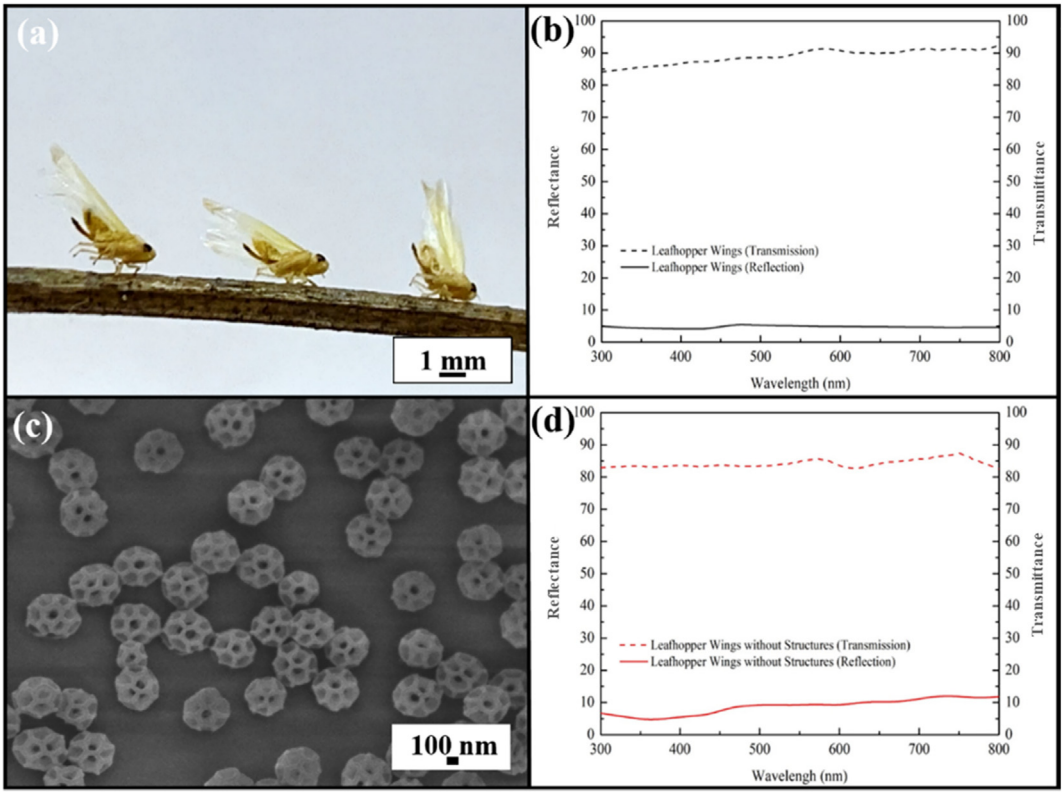

Fig. 2. (a) Photographic image of leafhoppers under white light illumination. (b) Visible reflectance and visible transmittance spectra of the leafhopper wings at normal incidence. (c) SEM image of the leafhopper wings in (a). (d) Visible reflectance and visible transmittance spectra of the leafhopper wings after removing the embroidered ball-like structures at normal incidence.

antireflective properties are studied as a prototype. Submicrometer-scale close-packed embroidered ball-like polymeric structures, whose structural geometry mimic the brochosomes, are self-assembled *via* a modified Langmuir-Blodgett technology. The as-fabricated structure shapes are turnable, allowing us to systemically investigate the effect of structural geometry on antireflective properties.

2. Experimental section

2.1. Materials and substrates

Leafhopper specimens are received from Muh Sheng Museum of Entomology. The reagents introduced for spherical silica colloid synthesis include tetraethyl orthosilicate (97 vol%, Sigma-Aldrich) and ammonium hydroxide (29 vol%, Sigma-Aldrich). Anhydrous ethanol (200 proof) is obtained from Echochemical Corporation. Ultrapure deionized water is purified in a Milli-Q system. Ethoxylated

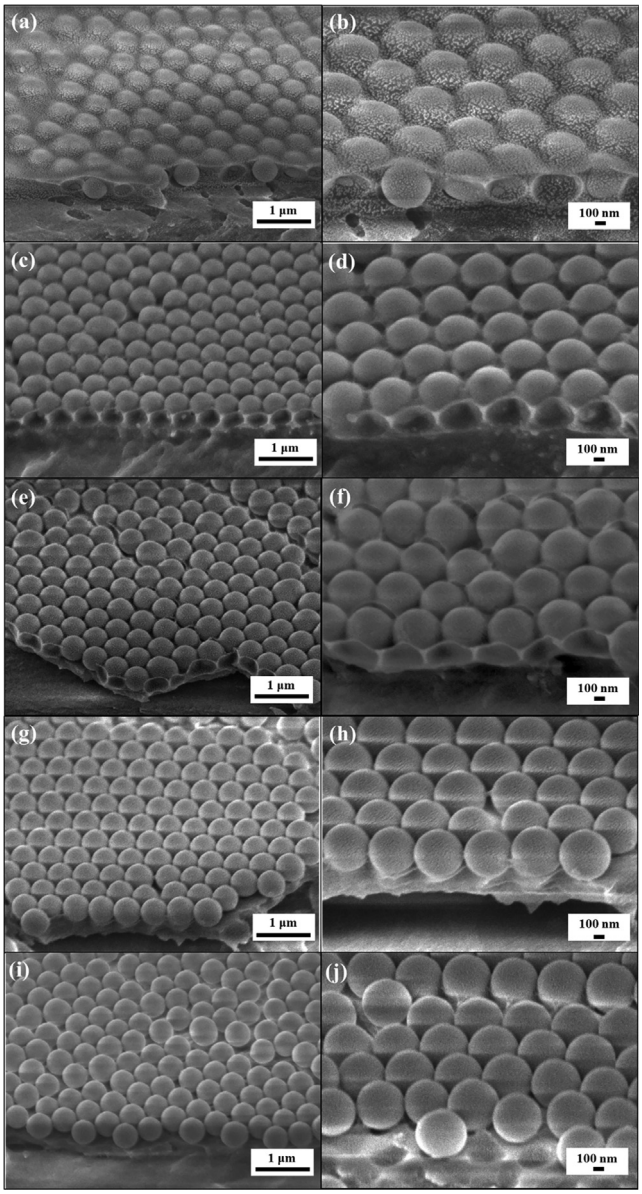

Fig. 3. SEM images of monolayer silica colloidal crystals fabricated by applying 500 nm silica colloidal suspensions with various silica colloid volume fractions. (a), (b) 20 vol%, (c), (d) 25 vol%, (e), (f) 30 vol%, (g), (h) 35 vol%, and (i), (j) 40 vol%.

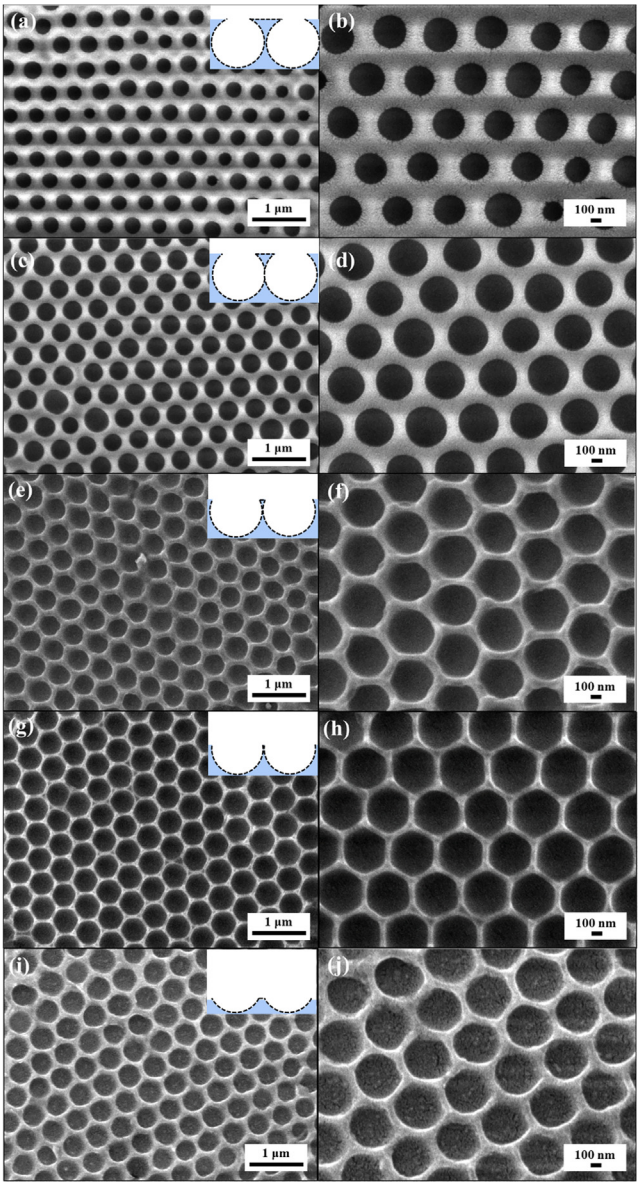

Fig. 4. SEM images of hole arrays fabricated by applying 500 nm silica colloidal suspensions with various silica colloid volume fractions. (a), (b) 20 vol%, (c), (d) 25 vol%, (e), (f) 30 vol%, (g), (h) 35 vol%, and (i), (j) 40 vol%.

trimethylolpropane triacrylate (ETPTA) (SR 454, Sartomer Company Corporation) monomer, and ethylene glycol diacrylate (EGDA) (SR 610, Sartomer Company Corporation) monomer, and photoinitiator, 2-hydroxy-2-methyl-1-phenyl-1-propanone (Darocur 1173, BASF Corporation), are used directly in this study. Poly(ethylene terephthalate) (PET) films (0.01 cm in thickness) acquired from Wisegate Technology are rinsed with anhydrous ethanol before use.

2.2. Preparation of StÖber silica colloidal suspensions

Monodispersed silica colloids with varied diameters (500 nm, 210 nm, 140 nm, and 90 nm) are prepared using StÖber method [33]. The as-synthesized StÖber silica colloids are cleaned using anhydrous ethanol by repeating centrifugation-dispersion procedure for three cycles, followed by dispersing the silica colloids in a ETPTA monomer/Darocur 1173 (1 vol%) mixture.

2.3. Langmuir-Blodgett assembly of close-packed hole arrays

The procedure for fabricating artificial brochosome arrays utilizing a modified Langmuir-Blodgett technique is schematically illustrated in Fig. 1. In this procedure, a cleaned PET film is attached to a syringe pump (KD Scientific 780), and immersed in ultrapure deionized water. After filtration to remove aggregates, a 500 nm silica colloidal suspension is continuously dropped onto the water, while ETPTA monomer-covered silica colloids are self-assembled into monolayer close-packed arrangement, resulting from high surface tension of water [34]. The syringe pump is then employed to withdraw the PET film with a consistent speed of 1 cm/min, during which the floating silica colloidal crystals are uniformly transferred onto the PET film. The continuous self-assembly process allows only little structural difference between the early and late stages in colloid deposition. After photopolymerization of ETPTA monomers with UV exposure, the silica colloids are etched in a hydrofluoric acid solution (1 vol%) to bring out close-packed hole arrays.

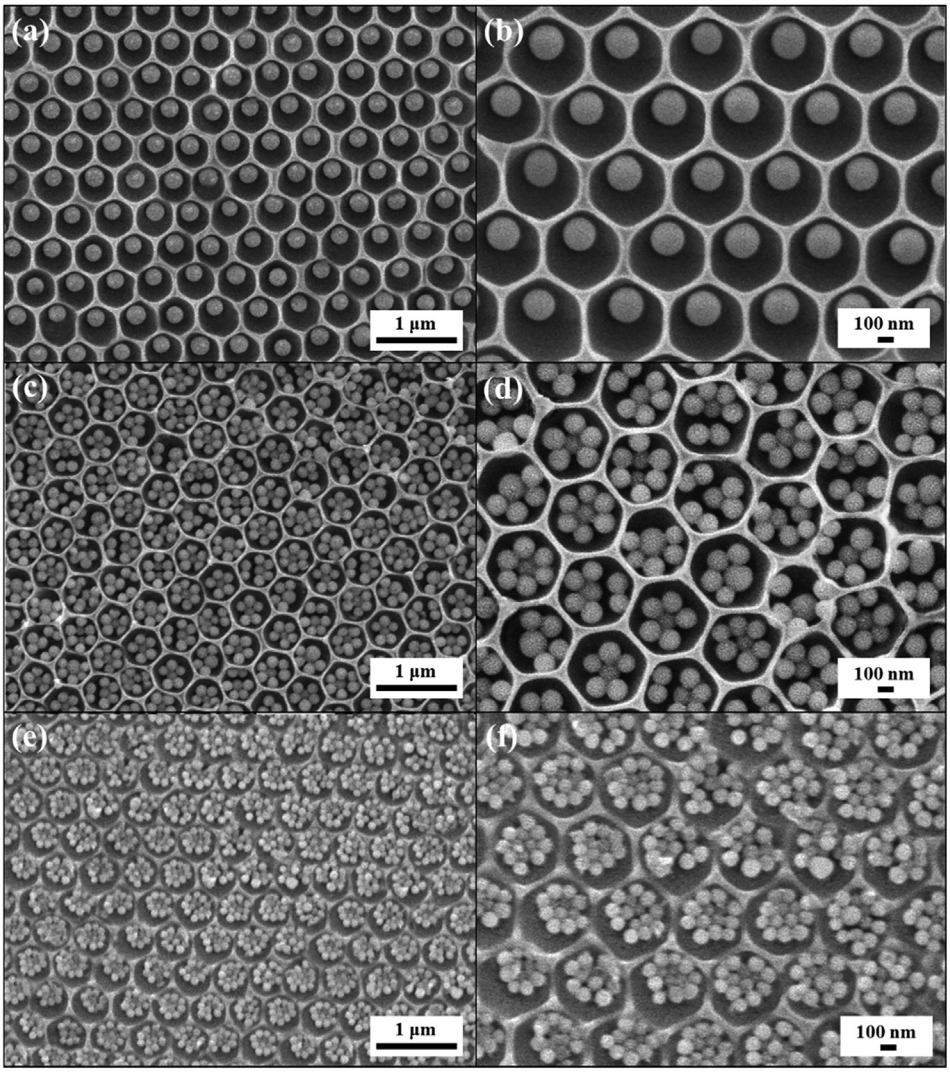

Fig. 5. SEM images of (a), (b) self-assembled 210 nm silica colloid crystals, (c), (d) self-assembled 140 nm silica colloid crystals, and (e), (f) self-assembled 90 nm silica colloid crystals onto the as-prepared 500 nm hole arrays.

2.4. Langmuir-Blodgett assembly of embroidered ball-like structure arrays

Subwavelength-scale silica colloids are subsequently Langmuir-Blodgett assembled and deposited onto the holes. In the deposition procedure, the coating speed is controlled to be 1 cm/min, during which 35 vol% silica colloidal suspensions are applied. The subwavelength-scale silica colloid-coated hole arrays can be utilized as second-generation patterns to engineer artificial brochosome arrays. In the molding process, an EGDA monomer/Darocur 1173 (1 vol%) mixture is cast onto the patterns, and then polymerized under UV illumination. After wet etching silica colloids, the embroidered ball-like structure-coated PEGDA films can be easily peeled off.

2.5. Characterization

Photographic images of the leafhoppers and PET substrates are conducted by a Nikon D5600 digital camera. The specimens are examined under a scanning electron microscopy (SEM, JEOL 6335F) for investigating the surface morphologies after sputtering a gold layer. Reflectance and transmittance spectra are carried out by a fiber-optic UV-visible-near-IR spectrometer (Ocean Optics HR4000) with a halogen tungsten light source, and recorded by Ocean Optical Spectra Suite Spectroscopy Software.

3. Results and discussion

For enhancing camouflage against avian predators, small yellow leafhopper wings exhibit a low haze under natural light illumination (Fig. 2(a)). To evaluate the optical characteristics of the leafhopper wings, visible reflectance and visible transmittance spectra are acquired as represented in Fig. 2(b). The average visible reflectance reaches *ca.* 4%, while an average visible transmittance of *ca.* 90% can be achieved. These broadband antireflection performances appear to result from the leafhopper-generated brochosomal coatings (Fig. 2(c)). The complex hierarchical constructions of brochosomes, submicrometer-scale granules covered with subwavelength-scale holes, establish a refractive index gradient on the leafhopper wing surface, and therefore reducing incident light reflection. Importantly, after removing the non-sticky brochosomal coatings under sonication in an ultrasonic bath (40 kHz/400 Watts) with water for 30 min, the leafhopper wings display *ca.* 5% higher average reflectance and *ca.* 6% lower average transmittance (Fig. 2(d)). The findings provide evidence for the antireflective function of brochodomes.

Inspired by the brochosomes on leafhopper wings, embroidered ball-like structure arrays are developed through combining a modified Langmuir-Blodgett technology and a soft lithography method. In the fabrication process, ETPTA monomer-covered 500 nm silica colloids are self-assembled and deposited on a PET substrate. The flowable ETPTA

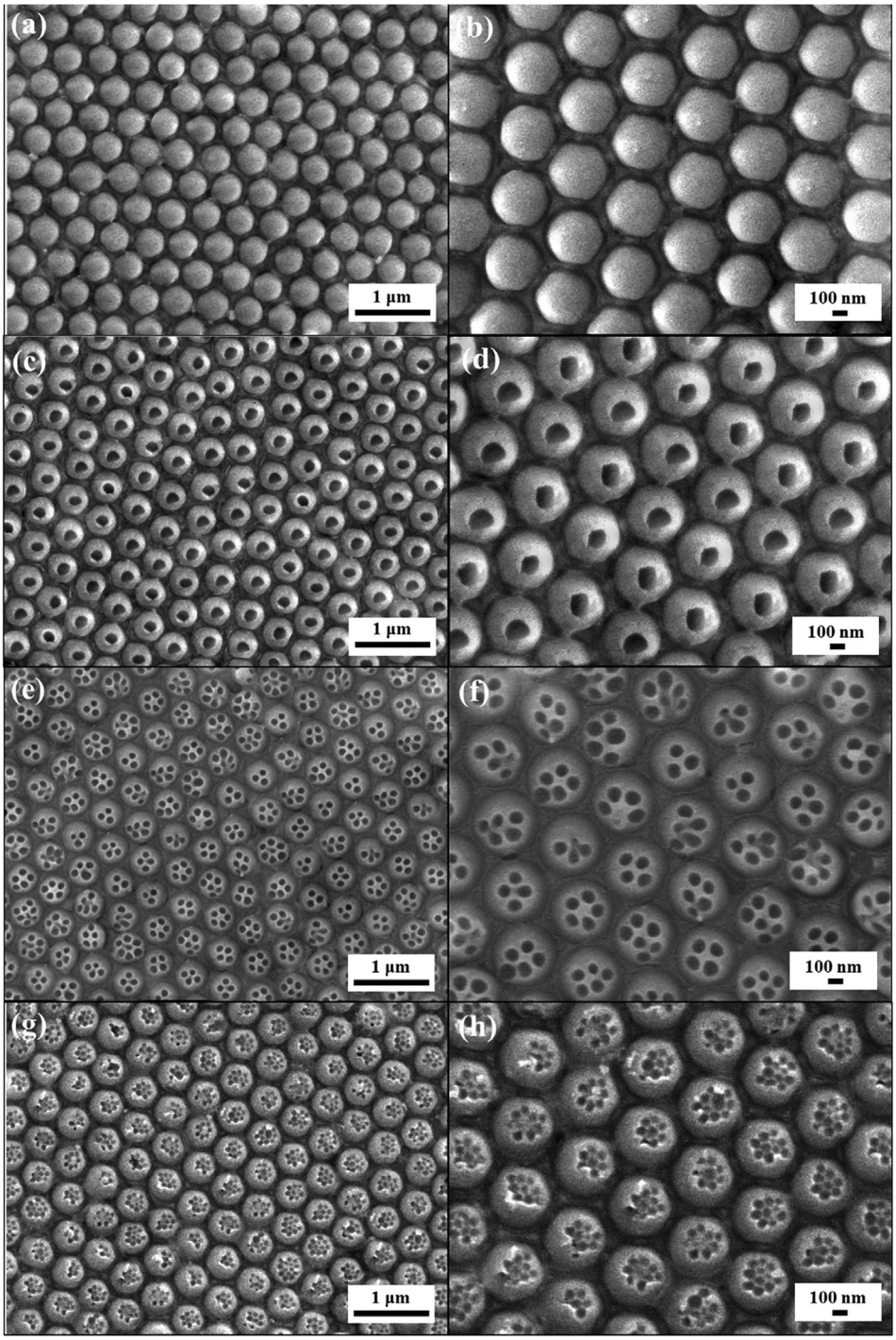

Fig. 6. SEM images of (a), (b) dome arrays, and artificial brochosome arrays covered with (c), (d) 210 nm holes, (e), (f) 140 nm hole arrays, and (g), (h) 90 nm hole arrays.

monomers slowly fill the space between the silica colloids and the substrate, which is attributed to gravity and capillary forces. After polymerization of ETPTA monomers, the close-packed silica colloidal crystals with long-range orderings are clearly revealed in Fig. 3. Importantly, introducing of silica colloidal suspensions with higher colloidal volume fractions leads to less polymer-embedded silica colloidal crystals. The silica colloids are subsequently wet etched to create 500 nm hole arrays (Fig. 4). Even through a few defects are observed, hexagonal ordering of the constituting holes is retained. The SEM images further disclose that the hole size increases with increasing of colloidal volume fraction. Furthermore, top silica hemispheres are fully exposed, and the silica templates results in the formation of maximum-sized close-packed hole arrays (*ca.* 500 nm in average) as a 35 vol% silica colloidal suspension is applied.

Subwavelength ETPTA monomer-covered silica colloids (210 nm, 140 nm, and 90 nm) are then self-assembled and transferred onto the 500 nm hole arrays using the modified Langmuir-Blodgett approach. After polymerization, the silica colloidal crystals are partial embedded in the polymeric matrix and attached to the holes, whereas the monomers function as adhesives during the process. As represented in Fig. 5, close-packed arrangements of the monolayer subwavelength silica colloidal crystals are well preserved, resulting from the capillary forces

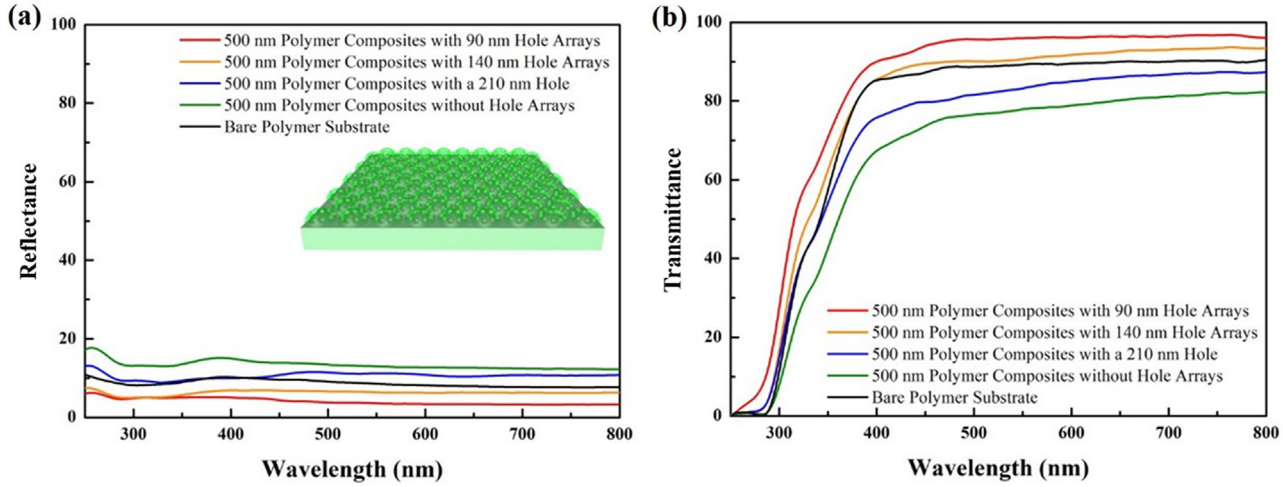

Fig. 7. (a) Visible reflectance spectra and (b) visible transmittance spectra of a bare PET film and PET films coated with artificial brochosome arrays, which covered with varied hole arrays, at normal incidence.

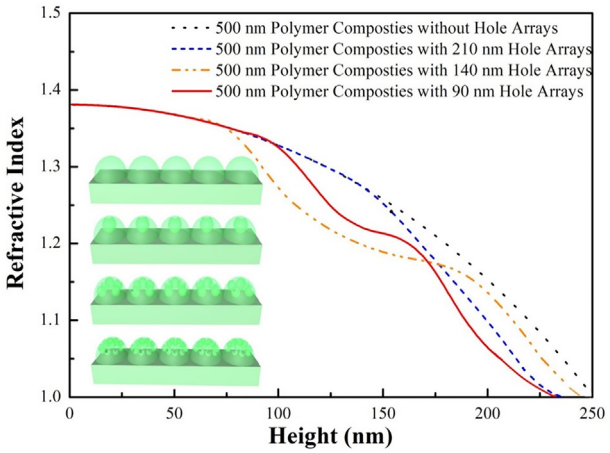

Fig. 8. The changes of calculated effective refractive indexes from PET films (height = 0) to the tops of templated artificial brochosomes.

between silica colloids and the high flexibility of floating silica colloidal crystals on the water surface. It is worth noting that the average depth of the holes is *ca.* 250 nm, and thus the space is only available for deposition of single 210 nm silica colloid. The silica deposited hole arrays are utilized as second-generation molds by which PEGDA oligomers with appropriate amount are casted and sandwiched between the molds and cleaned PET substrates, following by UV exposure for polymerization. The hexagonal orderings of the resulting PEGDA embroidered ball-like structures are well retained after peeling off the molds (Fig. 6). Compared with the dome arrays (Fig. 6(a) and (b)) templated from featureless hole arrays, subwavelength holes are engineered on the artificial brochosome arrays (Fig. 6(c)–(h)) using silica-deposited hole arrays as molds. In addition, the surface morphologies of the structures can be determined by applying varied silica colloidal crystals. Importantly, the subwavelength silica colloids are embedded and anchored on the molds throughout the replication process.

To assess antireflective properties of the leafhopper wing-inspired artificial brochosome arrays, normal incidence optical spectra of a bare PET film and artificial brochosome-coated PET films are measured and compared in Fig. 7. With discontinue refractive index transition on the featureless PET film, the specimen (black curves) exhibits an average reflectance of *ca.* 9% and an average transmittance of *ca.* 86% in the whole visible spectrum, complying with previous research [11]. Interestingly, the dome array-coated specimen (green curve) displays even higher reflectance and lower transmittance in the same wavelength range, which are caused by incidence visible light reflection from

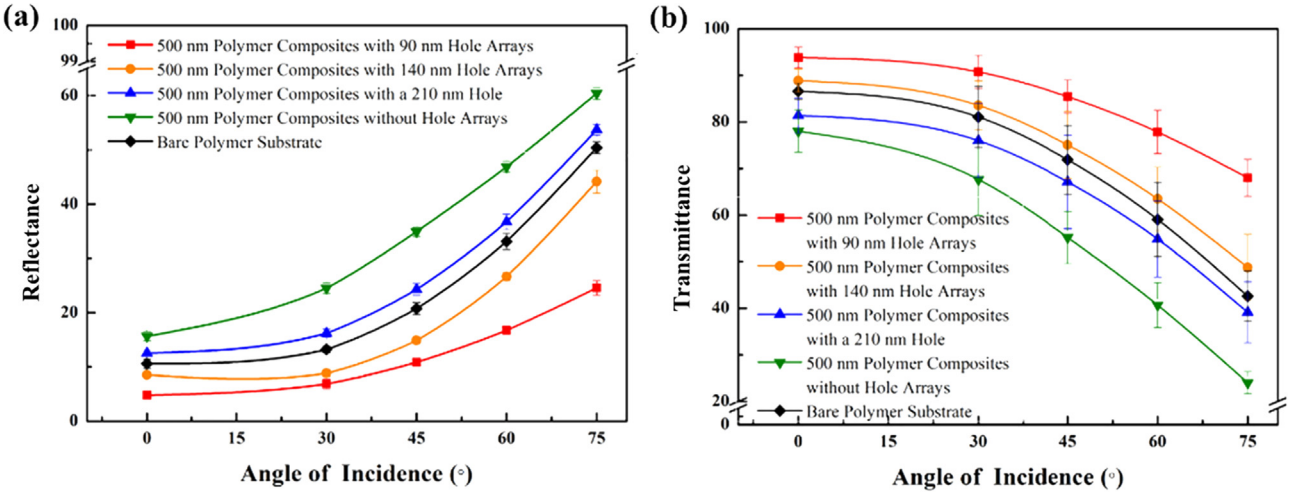

Fig. 9. (a) Average visible reflectance spectra and (b) average visible transmittance spectra of a bare PET film and PET films coated with artificial brochosome arrays, which covered with varied hole arrays, at various incidence angles.

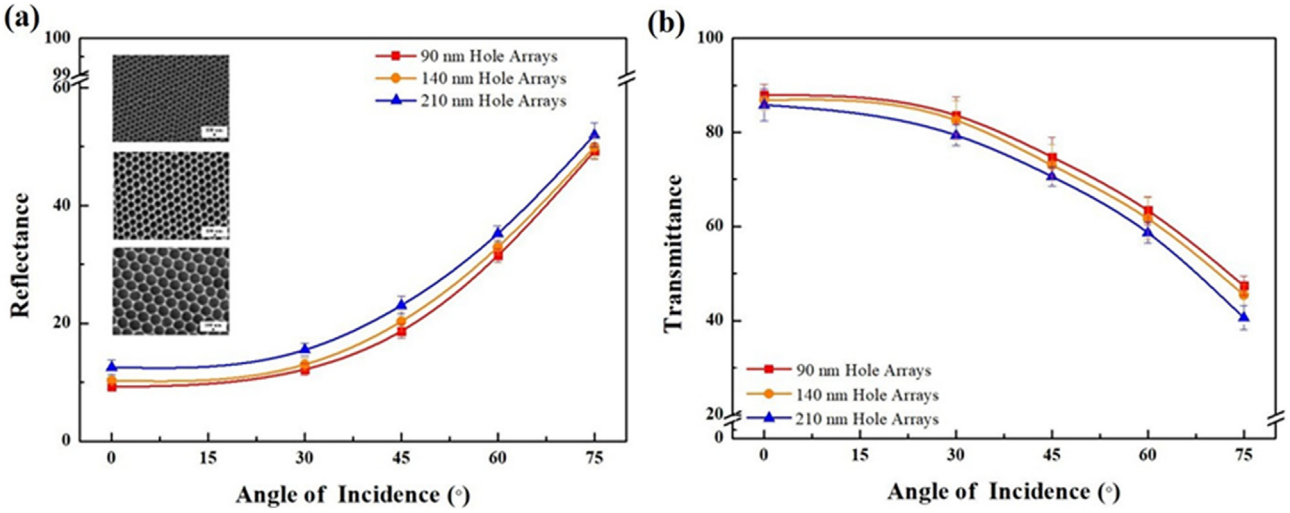

Fig. 10. (a) Average visible reflectance spectra and (b) average visible transmittance spectra of PET films coated with varied hole arrays at various incidence angles.

Fig. 11. Photographic images of PET films with the left half coated with (a) artificial brochosome arrays covered with 90 nm hole arrays, and (b) 90 nm hole arrays.

500 nm domes and light refraction within the domes. Compared with that, the visible reflectance of PET films can be reduced by introducing embroidered ball-like structures arrays. Importantly, less incident light is scattered from smaller subwavelength holes, and therefore the embroidered ball-like structures covered with smaller holes exhibit lower specular reflectance and higher specular transmittance in the visible spectrum. It is evident that the reflectance of 90 nm hole-covered artificial brochosome-coated specimen reaches *ca.* 4%, while the transmittance of *ca.* 94% is achieved. The broadband antireflection performance of hierarchical structures is further interpreted by mapping calculated effective refractive index transition from the top of embroidered ball-like structure (height = 250 nm) to the substrate (height = 0 nm) (Fig. 8), which governs the incident light propagation. Compared with other dotted curves, the 90 nm hole-covered artificial brochosome arrays possess lower average refractive index across the height of embroidered ball-like structure and smoother refractive index transition at the air/structure interface (height = 250 nm), and thus suppress specular reflectance in the visible spectrum more efficiently.

In order to comprehend the structure shape effect on the omnidirectional antireflective property, the visible reflectance spectra and visible transmittance spectra of a bare PET film and artificial brochosome-coated PET films are evaluated at various incidence angles (Figure S1) and summarized in Fig. 9. It is found that the average visible reflectances of all the specimens mentioned above increase as the incidence angle increases from 0 to 75°. Although introduction of 500 nm domes leads to higher average reflectance at various incidence angles, it is clear that smaller hole-covered embroidered ball-like structures can significantly suppress visible reflection for large incidence angles. The average visible reflectance of the 90 nm hole-covered artificial brochosome-coated PET film reaches *ca.* 5% at 0°, while the average visible reflectance of that reaches *ca.* 24% at 75° (red curve). Importantly, the average visible transmittances of the specimens display similar tendencies. In comparison with a bare film (black curve), the average visible transmittance can be improved by *ca.* 24% at 75° as 90 nm hole-covered artificial brochosome arrays are created (red curve). The broadband omnidirectional antireflection performance can be expressed by comparing the refractive index transitions across the structures at 15°, 30°, 45°, 60°, and 75° (Figure S2). In comparison with other structures, the 90 nm hole-covered artificial brochosomes possess lower refractive index and smoother refractive index transition at various incidence angles, resulting in better broadband omnidirectional antireflective capabilities.

This research further investigates the dependence of subwavelength hole arrays on the omnidirectional antireflective property. Monolayer hemispherical hole arrays with varied hole sizes are self-assembled on PET films directly according to the as-mentioned modified Langmuir-Blodgett approach. As displayed in the inserts of Fig. 10(a), hexagonal ordering of close-packed 210 nm hole arrays, 140 nm hole arrays, and 90 nm hole arrays can be achieved. The visible reflectance spectra and visible transmittance spectra of hole array-coated PET films at various incidence angles are disclosed in Figure S3 and summarized in Fig. 10. Owing to smaller hole size and inter-hole distance, less incident light is reflected on the 90 nm hole surface or lost within the hole after internal reflections. Therefore, the 90 nm hole array-coated PET substrate is with lower average reflectances and higher average transmittances in the visible wavelength region at various incidence angles. The average transmittance of the 90 nm hole-coated specimen reaches *ca.* 87% at 0°, while the average transmittance of that reaches *ca.* 48% at 75°, which

are slightly higher than these of a bare specimen (Fig. 9(b)). Compared with that, the average transmittances at various incidence angles can be further improved by introducing 90 nm hole-covered artificial brochosomes. The hierarchical structures provide more moderate effective refractive index transition, leading to superior omnidirectional antireflection performance.

The photographic images of PET substrates coated with 90 nm hole-covered artificial brochosome arrays and 90 nm hole arrays illuminated with white light are presented in Fig. 11(a) and (b), respectively. In contrast to the strong optical reflection on the featureless substrate (Fig. 11(a), right), the embroidered ball-like structure-coated substrate (Fig. 11(a), left) is highly transparent and uniform, indicating that the optical reflection is considerably reduced even though a few defects are observed in Fig. 6. Additionally, compared with the embroidered ball-like structure-coated substrate, it is evident that the hole array-coated substrate (Fig. 11(b), left) exhibits a lower transparency and some haze. The results further confirm that embroidered ball-like structure arrays perform higher broadband antireflective properties than hole arrays.

4. Conclusions

In summary, this research develops a non-photolithography-based methodology to engineer artificial brochosome arrays, which are inspired by the leafhopper-generated hierarchical constructions of brochosomes. The optical analyses reveal that incident light reflection is significantly suppressed by introducing embroidered ball-like structures. Furthermore, the as-fabricated sub-100 nm hole-covered artificial brochosome-coated film displays a higher transparency and improved broadband antireflection capability for wide viewing angles, which are promising for a variety of optical applications.

CRediT authorship contribution statement

Meng-Shan Shih: Methodology, Validation, Investigation, Resources, Writing - original draft. **Huei-Yin Chen:** Software, Investigation, Visualization. **Pei-Chun Li:** Software, Investigation, Resources. **Hongta Yang:** Conceptualization, Writing - review & editing, Supervision, Project administration, Funding acquisition.

Declaration of Competing Interest

The authors declare that they have no known competing financial interests or personal relationships that could have appeared to influence the work reported in this paper.

Acknowledgement

Acknowledgment is made to National Science Council, Taiwan (MOST 108-2221-E-005-038-MY2.) for supporting this study.

Appendix A. Supplementary data

Supplementary data to this article can be found online at https://doi.org/10.1016/j.apsusc.2020.147397.

References

[1] M. Ottaviani, J. Chowdhary, B. Cairns, Remote Sensing of the Ocean Surface Refractive Index Via Short-Wave Infrared Polarimetry, Remote Sens. Environ. 221 (2019) 14–23.
[2] F. Chi, D. Liu, H. Wu, J. Lei, Mechanically Robust and Self-Cleaning Antireflection Coatings from Nanoscale Binding of Hydrophobic Silica Nanoparticles, Sol. Energy Mater. Sol. Cells 200 (2019) 109939.
[3] C. Hudaya, B.J. Jeon, A. Verdianto, J.K. Lee, Y.-E. Sung, Antiglare and Antireflective Coating of Layer-By-Layer SiO_2 and $TiZrO_2$ on Surface-Modified Glass, Appl. Surf. Sci. 490 (2019) 278–282.
[4] Z. Meng, B. Huang, S. Wu, L. Li, S. Zhang, Bio-Inspired Transparent Structural Color Film and Its Application in Biomimetic Camouflage, Nanoscale 11 (2019) 13377–13384.
[5] S. Cheeseman, V.K. Truong, V. Walter, F. Thalmann, C.M. Marques, E. Hanssen, J. Vongsvivut, M.J. Tobin, V.A. Baulin, S. Juodkazis, S. Maclaughlin, G. Bryant, R.J. Crawford, E.P. Ivanova, Interaction of Giant Unilamellar Vesicles with the Surface Nanostructures on Dragonfly Wings, Langmuir 35 (2019) 2422–2430.
[6] Y.-C. Chen, Z.-S. Huang, H. Yang, Cicada-Wing-Inspired Self-Cleaning Antireflection Coatings on Polymer Substrates, ACS Appl. Mater. Interf. 7 (2015) 25495–25505.
[7] R.H. Siddique, G. Gomard, H. Hölscher, The Role of Random Nanostructures for the Omnidirectional Anti-Reflection Properties of the Glasswing Butterfly, Nat. Commun. 6 (2015) 6909.
[8] K. Askar, Z. Gu, C.J. Leverant, J. Wang, C. Kim, B. Jiang, P. Jiang, Self-Assembled Nanoparticle Antireflection Coatings on Geometrically Complex Optical Surfaces, Opt. Lett. 43 (2018) 5238–5241.
[9] Q. Ding, Y. Kang, W. Li, G. Sun, H. Liu, M. Li, Z. Ye, M. Zhou, J. Zhou, S. Yang, Bioinspired Brochosomes as Broadband and Omnidirectional Surface-Enhanced Raman Scattering Substrates, J. Phys. Chem. Lett. 10 (2019) 6484–6491.
[10] Z. Han, Z. Wang, B. Li, X. Feng, Z. Jiao, J. Zhang, J. Zhao, S. Niu, L. Ren, Flexible Self-Cleaning Broadband Antireflective Film Inspired by the Transparent Cicada Wings, ACS Appl. Mater. Interf. 11 (2019) 17019–17027.
[11] C.-Y. Lin, K.-Y.-A. Lin, T.-W. Yang, Y.-C. Chen, H. Yang, Self-Assembled Hemispherical Nanowell Arrays for Superhydrophobic Antireflection Coatings, J. Colloid Interf. Sci. 490 (2017) 174–180.
[12] W.L. Min, B. Jiang, P. Jiang, Bioinspired Self-Cleaning Antireflection Coatings, Adv. Mater. 20 (2008) 3914–3918.
[13] J. Morikawa, M. Ryu, G. Seniutinas, A. Balčytis, K. Maximova, X. Wang, M. Zamengo, E.P. Ivanova, S. Juodkazis, Nanostructured Antireflective and Thermoisolative Cicada Wings, Langmuir 32 (2016) 4698–4703.
[14] X. Zhang, J. Zhang, Z. Ren, X. Li, X. Zhang, D. Zhu, T. Wang, T. Tian, B. Yang, Morphology and Wettability Control of Silicon Cone Arrays Using Colloidal Lithography, Langmuir 25 (2009) 7375–7382.
[15] T. Yanagishita, K. Nishio, H. Masuda, Anti-Reflection Structures on Lenses by Nanoimprinting Using Ordered Anodic Porous Alumina, Appl. Phys. Exp. 2 (2009) 022001.
[16] F. Wu, G. Shi, H. Xu, L. Liu, Y. Wang, D. Qi, N. Lu, Fabrication of Antireflective Compound Eyes by Imprinting, ACS Appl. Mater. Interf. 5 (2013) 12799–12803.
[17] J. Sun, X. Wang, J. Wu, C. Jiang, J. Shen, M.A. Cooper, X. Zheng, Y. Liu, Z. Yang, D. Wu, Biomimetic Moth-Eye Nanofabrication: Enhanced Antireflection with Superior Self-Cleaning Characteristic, Sci. Rep. 8 (2018) 5438.
[18] V.V. Pradeep, M. Annadhasan, R. Chandrasekar, Vapour-Phase Epitaxial Growth of Dual-Colour-Emitting DCM-Perylene Micro-Heterostructure Optical Waveguides, Chem. Asian J. 14 (2019) 4577–4581.
[19] T. Bottein, T. Wood, T. David, J.B. Claude, L. Favre, I. Berbézier, A. Ronda, M. Abbarchi, D. Grosso, "Black" Titania Coatings Composed of Sol-Gel Imprinted Mie Resonators Arrays, Adv. Funct. Mater. 27 (2017) 1604924.
[20] Y. Yang, T. Wang, T. Yao, G. Li, Y. Sun, X. Cao, L. Ma, S. Peng, Preparation of a Novel TiN/TiNxOy/SiO2 Composite Ceramic Films on Aluminum Substrate as a Solar Selective Absorber by Magnetron Sputtering, J. Alloys Compd. 152209 (2019).
[21] S.B. Khan, Z.J. Zhang, S.L. Lee, Annealing Influence on Optical Performance of HfO_2 Thin Films, J. Alloys Compd. 4 (2017) 177–181.
[22] Y.-F. Huang, S. Chattopadhyay, Y.-J. Jen, C.-Y. Peng, T.-A. Liu, Y.-K. Hsu, C.-L. Pan, H.-C. Lo, C.-H. Hsu, Y.-H. Chang, Improved Broadband and Quasi-Omnidirectional Anti-Reflection Properties with Biomimetic Silicon Nanostructures, Nat. Nanotechnol. 2 (2007) 770.
[23] R. Rakitov, S.N. Gorb, Brochosomes Protect Leafhoppers (Insecta, Hemiptera, Cicadellidae) from Sticky Exudates, J. R. Soc. Interf. 10 (2013) 20130445.
[24] M. Tabe, M. Kumezawa, T. Yamamoto, S. Makita, T. Yamaguchi, Y. Ishikawa, Formation of High-Density Silicon Dots on a Silicon-on-Insulator Substrate, Appl. Surf. Sci. 142 (1999) 553–557.
[25] G.A. Ozin, S.M. Yang, The Race for the Photonic Chip: Colloidal Crystal Assembly in Silicon Wafers, Adv. Funct. Mater. 11 (2001) 95–104.
[26] R. Rakitov, S.N. Gorb, Brochosomes Protect Leafhoppers (Insecta, Hemipera, Cicadellidae) from Sticky Exudates, J. R. Soc. Interface 10 (2013) 20130445.
[27] Q. Pan, H. Zhang, Y. Yang, C. Cheng, 3D Brochosomes-Like $TiO_2/WO_3/BiVO_4$ Arrays as Photoanode for Photoelectrochemical Hydrogen Production, Small 1900924 (2019).
[28] Q. Ding, Y. Kang, W. Li, G. Sug, H. Liu, M. Li, Z. Ye, M. Zhou, J. Zhou, S. Yang, Bioinspired Brochosomes as Broadband and Omnidirectional Surface-Enhanced Raman Scattering Substrates, J. Phys. Chem. Lett. 10 (2019) 6484–6491.
[29] R. Sukamanchi, D. Mathew, S. Kumar, Durable Superhydrophobic Particles Mimicking Leafhopper Surface: Superoleophilicity and Very Low Surface Energy, ACS Sustain. Chem. Eng. 5 (2017) 252–260.
[30] A.K. Singh, J.K. Singh, Fabrication of durable Super-Repellent Surfaces on Cotton Fabric with Liquids of Varying Surface Tension: Low Surface Energy and High Roughness, Appl. Surf. Sci. 418 (2017) 639–648.
[31] L. Borja, Synthesis Replicates Camouflaging-Brochosome Particle Structure, MRS Bull. 43 (2018) 10.
[32] S. Yang, N. Sun, B.B. Stogin, J. Wang, Y. Huang, T.-S. Wong, Ultra-Antireflective Synthetic Brochosomes, Nat. Commun. 8 (2017) 1285.
[33] W. Stöber, A. Fink, E. Bohn, Controlled Growth of Monodisperse Silica Spheres in the Micron Size Range, J. Colloid Interf. Sci. 26 (1968) 62–69.
[34] C.-Y. Lin, K.-Y. Lin, H.-P. Tsai, Y.-X. He, H. Yang, Self-Assembled Dual-Sided Hemispherical Nano-Dimple-Structured Broadband Antireflection Coatings, Appl. Phys. Lett. 109 (2016) 221601.